

LORENTZ RESONANCE IN THE HOMOGENIZATION OF PLASMONIC CRYSTALS

WEI LI*, ROBERT LIPTON†, AND MATTHIAS MAIER‡

Abstract. We explain the sharp Lorentz resonances in plasmonic crystals that consist of 2D nano dielectric inclusions as the interaction between resonant material properties and geometric resonances of electrostatic nature. One example of such plasmonic crystals are graphene nanosheets that are periodically arranged within a non-magnetic bulk dielectric. We identify local geometric resonances on the length scale of the small scale period. From a materials perspective, the graphene surface exhibits a dispersive surface conductance captured by the Drude model. Together these phenomena conspire to generate Lorentz resonances at frequencies controlled by the surface geometry and the surface conductance.

The Lorentz resonances found in the frequency response of the effective dielectric tensor of the bulk metamaterial is shown to be given by an explicit formula, in which material properties and geometric resonances are decoupled. This formula is rigorous and obtained directly from corrector fields describing local electrostatic fields inside the heterogeneous structure.

Our analytical findings can serve as an efficient computational tool to describe the general frequency dependence of periodic optical devices. As a concrete example, we investigate two prototypical geometries composed of nanotubes and nanoribbons.

1. Introduction. Novel frequency dependent electromagnetic behavior can be generated by patterned dispersive dielectric metamaterials undergoing localized geometric resonance. Examples include plasmonic metasurfaces [27, 28], band gaps generated by periodic configurations of local plasmon resonators [21], and beam steering [18]. In this work we contribute to the *analytic* understanding of such periodic optical devices by investigating the role of local (frequency independent) geometric features and (frequency dependent) material properties. In particular, we explain the appearance of sharp Lorentz resonances generated by periodically patterned dispersive dielectrics *as the interaction* between resonant material properties and local geometric resonances of electrostatic nature.

Concretely, we shall examine the optical frequency response of plasmonic crystals formed by 2D material inclusions (such as graphene) embedded in a non-magnetic bulk dielectric host. We use a Drude model for the local conductivity response of the 2D material but allow for a fairly general periodic geometry including, for example, graphene nanoribbons, or graphene nanotubes. In such geometries, frequency independent geometric resonances will be identified and characterized that occur on the length scale of the period of the 2D material inclusions. These local resonances are novel as they exist both on the surface of the sheets and in the bulk. Together with the dispersive surface conductance of the 2D material, both phenomena conspire to generate Lorentz resonances in the effective optical frequency response of the metamaterial. The resonance frequencies are controlled by the surface geometry and the surface conductance.

The Lorentz resonances for the effective dielectric tensor or equivalently the effective index of refraction for the bulk metamaterial are shown to be given by an explicit formula. This formula is rigorous and obtained directly from corrector fields describing local electrostatic fields inside the heterogeneous structure. The local boundary value problem for the correctors follow from the periodic homogenization theory for Maxwell's equations developed in [1, 12, 22–24]. The formula for the effective di-

*Department of Mathematical Sciences, DePaul University, Chicago, IL 60614, USA

†Department of Mathematics, Louisiana State University, Baton Rouge, LA 70803, USA

‡Department of Mathematics, Texas A&M University, College Station, TX 77843, USA.

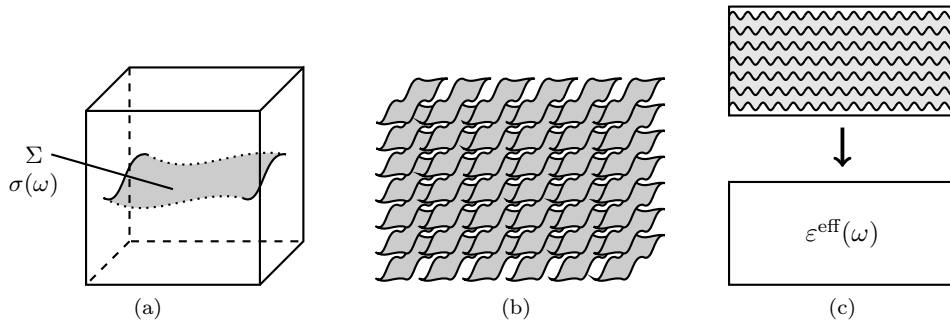


Figure 1: The homogenization procedure: (a) the nanoscale unit cell Y consisting of 2D metallic inclusions Σ with surface conductivity $\sigma(\omega)$ in an ambient host material with permittivity ε ; (b) the plasmonic crystal formed by many scaled and repeated copies of Y in every space dimension; (c) a schematic of the homogenization process in which the nanoscale structure is replaced by a homogeneous material with effective permittivity ε^{eff} .

electric constant obtained here is notable in that the local geometric resonances and local surface conductivity are uncoupled. This offers the opportunity for efficient computation of the effective dielectric constant through the computation of the local geometric resonances that are independent of the specific material properties. The interaction between geometry and material dispersion is displayed explicitly in the rigorously derived formula.

In detail, our contributions with the current work can be summarized as follows:

- We describe the interplay between frequency-independent geometric nanoscale resonances and frequency-dependent local conductivity models that results in Lorentz resonances in the effective optical frequency response. We derive an explicit formula for the frequency response rigorously from a mathematical homogenization theory for Maxwell’s equations for periodic 2D material inclusions.
- We discuss how to use the analytic result for computing approximations on the frequency response of periodic optical configurations. This approach offers a significant saving in computational resources because only one frequency-independent geometric eigenvalue problem has to be computed, in contrast to computing the corrector field for a huge number of fixed frequencies [12, 13].
- We examine two prototypical geometries—a nanotube, and a nanoribbon configuration—in more detail. The latter one is analytically and computationally much more challenging due to singularities at interior 2D material edges. We discuss decay estimates and examine the approximation quality of our computational approach.

1.1. Background: Homogenization of plasmonic crystals. The following analytical investigation is based on a rigorous periodic homogenization theory [1, 12, 22–24]. For the sake of simplicity, we will base our analytical investigation on a slightly simplified setting that we quickly outline here.

Consider a three-dimensional plasmonic crystal consisting of periodic copies of a *representative volume element* Y , which incorporates nanoscale inclusions given by

2D material surfaces (see Figure 1) of reasonably arbitrary shape (specified in Sec. 11.2 and Appendix A). The conductivity of the surfaces is assumed to obey the Drude model:

$$\sigma(\omega) = \frac{i\omega_p}{\omega + i/\tau},$$

where i denotes the imaginary unit, ω is the angular frequency, $\omega_p = 4\alpha \approx 4/137$ is a (rescaled) Drude weight, and τ is a material-dependent relaxation time. Here, we have non-dimensionalized all quantities by applying a convenient rescaling [11]: $\tilde{\omega} = \frac{\hbar\omega}{E_F}$, where E_F denotes the Fermi energy associated with the 2D material and \hbar is the reduced Planck constant; $\tilde{\sigma}(\tilde{\omega}) = \sqrt{\frac{\mu_0}{\varepsilon_0}} \sigma(\omega)$, where μ_0 and ε_0 denote the vacuum permeability and permittivity, respectively. We set the length, height, and width of the representative volume element to one, $Y = [0, 1]^3$. Furthermore, we assume that the dielectric host has a uniform and isotropic relative permittivity ε .

It can then be shown [12] that for sufficiently many repetitions of Y , i.e., a sufficiently large plasmonic crystal, the *effective* conductivity of the plasmonic crystal is given by a uniform, frequency-dependent conductivity tensor

$$(1.1) \quad \varepsilon_{ij}^{\text{eff}}(\omega) = \varepsilon \delta_{ij} - \frac{\sigma(\omega)}{i\omega} \int_{\Sigma} \{P_T(\mathbf{e}_j) + \nabla_T \chi_j(\omega, \mathbf{x})\} \cdot P_T(\mathbf{e}_i) d\mathbf{o}_x, \quad i, j = 1, 2, 3.$$

Here, δ_{ij} denotes Kronecker's Delta, \mathbf{e}_j is the j -th unit vector, Σ denotes the 2D material surface (embedded in Y), P_T is the projection of a vector onto the two-dimensional tangential space of Σ , and $\nabla_T = P_T \nabla$ denotes the tangential gradient (with respect to Σ). The Y -periodic corrector field $\chi(\mathbf{x})$ is the solution of the variational *cell problem* [12],

$$(1.2) \quad i\omega\varepsilon \int_Y \nabla \chi_j(\omega, \mathbf{x}) \cdot \nabla \overline{\psi(\mathbf{x})} dx - \sigma(\omega) \int_{\Sigma} \nabla_T \chi_j(\omega, \mathbf{x}) \cdot \nabla_T \overline{\psi(\mathbf{x})} d\mathbf{o}_x \\ = \sigma(\omega) \int_{\Sigma} P_T(\mathbf{e}_j) \cdot \nabla_T \overline{\psi(\mathbf{x})} d\mathbf{o}_x$$

which has to hold true for all admissible test functions ψ . Here, \bar{z} denotes the complex conjugate of a complex number z .

1.2. Summary of the main result. The objective of our discussion is to decouple the frequency dependence of (1.1) and (1.2) from the geometry. To this end we introduce an auxiliary spectral problem to identify all $\{\lambda_n\} \subset \mathbb{C}$ for which there exists a φ_n satisfying

$$(1.3) \quad \lambda_n \int_Y \nabla \varphi_n(\mathbf{x}) \cdot \nabla \overline{\psi(\mathbf{x})} dx = \int_{\Sigma} \nabla_T \varphi_n(\mathbf{x}) \cdot \nabla_T \overline{\psi(\mathbf{x})} d\mathbf{o}_x, \quad \int_{\Sigma} |\nabla_T \varphi_n(\mathbf{x})|^2 dx = 1,$$

for all admissible test functions ψ . Introducing $\eta(\omega) = \frac{\sigma(\omega)}{i\omega}$ we then show that the effective refractive index in (1.1) can be expressed by the formula

$$(1.4) \quad \varepsilon_{ij}^{\text{eff}}(\omega) = \varepsilon \delta_{ij} - \eta(\omega) \int_{\Sigma} P_T(\mathbf{e}_j) \cdot P_T(\mathbf{e}_i) d\mathbf{o}_x \\ - \sum_{n=1}^{\infty} \frac{\lambda_n \eta^2(\omega)}{\varepsilon - \lambda_n \eta(\omega)} \int_{\Sigma} P_T(\mathbf{e}_j) \cdot \nabla_T \overline{\varphi_k(\mathbf{x})} d\mathbf{o}_x \int_{\Sigma} \nabla_T \varphi_k(\mathbf{x}) \cdot P_T(\mathbf{e}_i) d\mathbf{o}_x.$$

The important property of this formula is that the integrals only depend on geometry, and the coefficients only depend on frequency. Equating the real part of the denominator in the coefficients of (1.4), viz., recovers an explicit resonance frequency $\omega_{R,n}$ for which the contribution of the n -th term of the sum may become dominant,

$$\omega_{R,n} = \sqrt{\omega_{0,n} - 1/(2\tau)^2}, \quad \text{where } \omega_{0,n} = \frac{\lambda_n \omega_p}{\varepsilon}, \quad n = 1, 2, \dots$$

The frequency dependent coefficient of the n -th term in the sum in (1.4) can be rewritten as

$$(1.5) \quad \frac{\lambda_n \eta^2(\omega)}{\varepsilon - \lambda_n \eta(\omega)} = \frac{\varepsilon \lambda_n \omega_p^2 (\omega - i/\tau)}{\omega(\omega^2 + 1/\tau^2)} \frac{(\omega_{0,n}^2 - \omega^2) + i\omega/\tau}{(\omega_{0,n}^2 - \omega^2)^2 + \omega^2/\tau^2}.$$

In general, we have $\omega \approx \omega + i/\tau$. For example, the relaxation time for graphene is approximately $\tau \approx 200$ [11]. Thus, close to a resonance frequency, viz., $\omega \approx \omega_{R,n}$, the first factor in (1.5) is approximately real valued and constant and the frequency dependence of the coefficient is entirely dominated by the second factor, which is Lorentzian.

1.3. Past works. The approach taken here is motivated by earlier observations of local resonances occurring at the length scale of the microgeometry. Electrostatic resonances identified at the length scale of composite geometry were shown to control the effective dielectric response associated with crystals made from non-dispersive dielectric inclusions in the pioneering work of [4] and [15]. The associated representation formulas based on local resonances were extended and applied to bound the effective dielectric response [16], [7], and [17]. Most recently local electrostatic and plasmonic resonances are used to construct non-magnetic double negative metamaterials in the near infrared [5] and design photonic band gap materials [9]. The current work advances the understanding of effective dielectric behavior by discovering and subsequently taking advantage of local resonances supported both on surfaces and in the bulk for generating sharp Lorentz resonances at frequencies explicitly controlled by the microstructure.

1.4. Paper organization. The remainder of the paper is organized as follows. In Section 2 we introduce the analytical setting and prove the main spectral decomposition result stated in Proposition 2.1. A computational framework based on the spectral decomposition is outlined in Section 3 and two prototypical geometries are computationally analyzed. We discuss implications and conclude in Section 4. Analytical technicalities concerning the spectral decomposition result on open surfaces is outlined in Appendix A. We summarize some explicit analytical formulas for the solution of the geometric eigenvalue problem in Appendix B.

2. Spectral Decomposition. In this section we formalize the spectral decomposition problem (1.3). For simplicity we restrict the discussion to geometries where the inclusion Σ is a *closed* Y -periodic surface, i.e., Σ does not have any edges in the interior of Y but might be periodically extended over the boundary of Y . In addition we require that the surface Σ is smooth enough to have a uniquely defined surface normal. For the case of *open* surfaces Σ , i.e., inclusions with internal edges, our main result (1.4) still holds, but requires some technical modifications that we spell out in detail in Appendix A. Note that the union of these two cases include a fairly general class of geometries for which characterization (1.4) is valid.

The appropriate function space for the variational problem (1.2) is

$$(2.1) \quad \mathcal{H} := \left\{ \psi \in H_{\text{per}}^1(Y, \mathbb{C}) : \nabla_T \psi \in L^2(\Sigma, \mathbb{C}), \int_Y \psi = 0 \right\}.$$

Here, $H_{\text{per}}^1(Y)$ denotes the Sobolev space of periodic functions u such that u and its first order (distributional) partial derivatives are square integrable in Y , and $L^2(\Sigma)$ denotes the space of square-integrable functions on Σ . The space \mathcal{H} equipped with the norm $\|\cdot\|_{\mathcal{H}}^2 = \|\nabla \cdot\|_Y^2 + \|\nabla_T \cdot\|_{\Sigma}^2$ (and the corresponding inner product) is a Hilbert space. It can be shown that the corrector problem (1.2) admits a unique solution $\chi_j \in \mathcal{H}$ by the Lax-Milgram Lemma [1, 12, 22-24]. Thus we need to solve the spectral problem (1.3) over the space \mathcal{H} , which is to find all pairs of eigenfunctions $\varphi \in \mathcal{H}$ and eigenvalues $\lambda \in \mathbb{R}$, such that

$$\lambda \int_Y \nabla \varphi \cdot \nabla \bar{\psi} \, dx = \int_{\Sigma} \nabla_T \varphi \cdot \nabla_T \bar{\psi} \, d\sigma_x \quad \text{for all } \psi \in \mathcal{H}.$$

We will show that this eigenvalue problem corresponds to an underlying self-adjoint, compact operator on a suitable function space defined over Σ . We first formally summarize the mechanism, and will then make the steps rigorous in the remainder of the section.

Every eigenfunction φ has a representation $\varphi = \mathbf{S}\gamma$, where γ is a density function defined on Σ and \mathbf{S} is the periodic single layer operator:

$$(2.2) \quad \mathbf{S}\gamma(x) := \int_{\Sigma_*} G_{\text{per}}(x-y)\gamma(y) \, d\sigma_y, \quad x \in Y.$$

Here, G_{per} is the periodic Green's function of the associated Laplace problem. The single layer potential satisfies

$$(2.3) \quad \Delta \mathbf{S}\gamma = 0 \quad \text{in } \Omega \setminus \Sigma, \quad [\partial_{\nu} \mathbf{S}\gamma] = \gamma \quad \text{on } \Sigma.$$

Here, ν is the unit outward normal of Σ at \mathbf{x} , and $[f](\mathbf{x})$ denotes the jump of a quantity f across the surface Σ along the normal direction of Σ , viz.,

$$[f](\mathbf{x}) := \lim_{\alpha \searrow 0} \left(f(\mathbf{x} + \alpha\nu) - f(\mathbf{x} - \alpha\nu) \right) \quad \text{for } \mathbf{x} \in \Sigma.$$

Substituting the representation $\varphi = \mathbf{S}\gamma$ into (1.3), we obtain an equivalent spectral problem for γ :

$$\lambda \int_Y \nabla \mathbf{S}\gamma \cdot \nabla \bar{\psi} \, dx = \int_{\Sigma} \nabla_T \mathbf{S}\gamma \cdot \nabla_T \bar{\psi} \, d\sigma_x, \quad \text{for all } \psi \in \mathcal{H}.$$

Integration by parts of the volume integral further transforms the eigenvalue problem to an eigenvalue problem described exclusively on Σ :

$$-\lambda \int_{\Sigma} \gamma \bar{\psi} \, d\sigma_x = \int_{\Sigma} \nabla_T S\gamma \cdot \nabla_T \bar{\psi} \, d\sigma_x \quad \text{for all } \psi \in \mathcal{H}.$$

Here, S is the single layer operator \mathbf{S} restricted to Σ . Writing $\xi = S\gamma$ and assuming invertibility of S , we obtain

$$-\lambda \int_{\Sigma} S^{-1}\xi \bar{\psi} \, d\sigma_x = \int_{\Sigma} \nabla_T \xi \cdot \nabla_T \bar{\psi} \, d\sigma_x, \quad \forall \psi \in \mathcal{H},$$

This can be rewritten in strong form as follows,

$$\lambda S^{-1}\xi = \Delta_T \xi, \quad -\Delta_T := \nabla_T \cdot \nabla_T.$$

Provided that Δ_T^{-1} exists as well we are lead to the eigenvalue problem

$$(2.4) \quad \Delta_T^{-1} S^{-1} \xi = \lambda^{-1} \xi.$$

We will establish that the inverses S^{-1} and Δ_T^{-1} exist and that the operator $\Delta_T^{-1} S^{-1}$ is compact and self adjoint on a proper Hilbert space

$$N(\Sigma) := \left\{ \xi \in H^1(\Sigma) : \int_{\Sigma} S^{-1} \xi \, do_x = 0. \right\}.$$

This guarantees the existence of a countable set of real numbers $\{\lambda_n^{-1}\}_n$ converging to zero with an associated orthonormal basis of eigenvectors $\{\xi_n\}_n$ of that Hilbert space. Note that, by design, ξ_n is precisely the restriction of φ_n as characterized by (1.3) to the surface Σ . A number of algebraic manipulations then shows the following result:

PROPOSITION 2.1 (Spectral decomposition). *Let χ_j be the solution of the cell problem (1.2). Let $\{\xi_n, \lambda_n^{-1}\}_n$ be the aforementioned orthonormal basis of eigenvectors of $N(\Sigma)$ with associated eigenvalues, which are rigorously defined in Corollary 2.5. Then there exists a sequence of coefficients $\{\alpha_j^n\}_n \in \ell_2(\mathbb{C})$, such that the corrector χ_j can be represented by*

$$(2.5) \quad \chi_j = \mathbf{S} S^{-1} \left(\sum_n \alpha_j^n \xi_n \right) + C.$$

The coefficients are given by

$$(2.6) \quad \alpha_j^n = \frac{\lambda_n \eta(\omega)}{\varepsilon - \lambda_n \eta(\omega)} \int_{\Sigma} P_T(\mathbf{e}_j) \cdot \nabla_T \bar{\xi}_k \, do_x.$$

Furthermore, the dielectric tensor takes the form

$$(2.7) \quad \varepsilon_{ij}^{\text{eff}} = \varepsilon \delta_{ij} - \eta(\omega) \int_{\Sigma} P_T(\mathbf{e}_j) \cdot P_T(\mathbf{e}_i) \, do_x \\ - \sum_n \frac{\lambda_n \eta^2(\omega)}{\varepsilon - \lambda_n \eta(\omega)} \int_{\Sigma} P_T(\mathbf{e}_j) \cdot \nabla_T \bar{\xi}_n \, do_x \int_{\Sigma} \nabla_T \xi_n \cdot P_T(\mathbf{e}_i) \, do_x.$$

2.1. A density representation of the corrector. We start the proof of Proposition 2.1 by characterizing the corrector $\chi_i \in \mathcal{H}$ given by (1.2) in terms of a density γ and the Y -periodic single layer potential \mathbf{S} . Recall that we have restricted the discussion to the case of Σ without internal edges in Y . In this case, the following two properties hold:

1. The restricted single layer operator $S : L^2(\Sigma) \rightarrow H^1(\Sigma)$ is a bounded, invertible operator with a bounded inverse.
2. The jump of in the normal derivative of the solution $\chi_i \in \mathcal{H}$ of the cell problem (1.2) on the surface, $[\partial_{\nu} \chi_j]_{\Sigma}$, is in $L^2(\Sigma)$, where $L^2(\Sigma)$ the space of square integrable functions on Σ .

A proof of (i) for the case of Lipschitz continuous Σ can be found in [14, Thm. 7.17], and property (ii) is a direct consequence of standard trace theorems [6] and property (i). Note that Properties (i) and (ii) do not hold when Σ is an open surface, in the sense that it has edges in the interior of Y . Starting from (ii), we set

$$\gamma := [\partial_\nu \chi_j] \in L^2(\Sigma, \mathbb{C}).$$

Recalling (2.3) we observe that the difference $\chi_j - \mathbf{S}\gamma$ belongs to $H_{\text{per}}^1(Y, \mathbb{C})$ and its distributional Laplacian is zero everywhere in Y . Therefore,

$$\chi_j = \mathbf{S}\gamma + C,$$

where C is a constant. This suggests the following lemma:

LEMMA 2.2. *For the corrector χ_j solving (1.2), there exists a unique $\gamma \in L^2(\Sigma, \mathbb{C})$ and a unique complex valued constant C , such that*

$$(2.8) \quad \chi_j = \mathbf{S}\gamma + C, \quad \text{with} \quad \int_{\Sigma} \gamma \, do_x = 0.$$

Proof. We have already established existence. For the uniqueness, assume that we have two representations for χ_j , viz. $\mathbf{S}\gamma_1 + C_1 = \mathbf{S}\gamma_2 + C_2$. This implies that $\mathbf{S}(\gamma_1 - \gamma_2)$ is a constant in Y , and thus

$$\gamma_1 - \gamma_2 = [\partial_\nu \mathbf{S}(\gamma_1 - \gamma_2)] = 0 \quad \text{on } \Sigma.$$

It follows that C_1 and C_2 are also identical. Finally, note that $\Delta \mathbf{S}\gamma = 0$ implies

$$(2.9) \quad \int_{\Sigma} \gamma \, do_x = \int_{\Sigma} [\partial_\nu \mathbf{S}\gamma] \, do_x = - \int_{Y \setminus \Sigma} \Delta \mathbf{S}\gamma \, dx = 0. \quad \square$$

2.2. A compact and self-adjoint operator. The property of the density function γ in Lemma 2.2 suggests that we work with the space

$$(2.10) \quad N(\Sigma) := \left\{ \xi \in H^1(\Sigma) : \int_{\Sigma} S^{-1} \xi \, do_x = 0 \right\}.$$

A straightforward calculation shows that $N(\Sigma)$ equipped with the seminorm $\|\nabla_T \xi\|_{L^2(\Sigma)}$ is a Hilbert space. The Riesz representation theorem then establishes a particular inverse of the Laplace-Beltrami operator Δ_T :

LEMMA 2.3. *For $f \in L^2(\Sigma)$ with $\int_{\Sigma} f \, do_x = 0$, there exists a unique $g \in N(\Sigma)$, such that*

$$\int_{\Sigma} \nabla_T g \cdot \nabla_T \bar{\psi} \, do_x = - \int_{\Sigma} f \bar{\psi} \, do_x, \quad \text{for all } \psi \in N(\Sigma).$$

Moreover, the solution g is bounded, viz., $\|\nabla_T g\|_{L^2(\Sigma)} \leq C \|f\|_{L^2(\Sigma)}$. We will denote this solution operator by Δ_T^{-1} .

We are now in a position to formulate and prove a central proposition and corollary.

PROPOSITION 2.4. *The operator*

$$\Delta_T^{-1} S^{-1} : N(\Sigma) \rightarrow N(\Sigma)$$

is compact and self-adjoint. Moreover, $\ker(\Delta_T^{-1} S^{-1}) = \{0\}$.

COROLLARY 2.5 (Spectrum). *The spectrum of $\Delta_T^{-1}S^{-1}$ consists of countably many nonzero eigenvalues $\{\lambda_n^{-1}\}_n$, only possibly accumulating at 0. The corresponding eigenfunctions $\{\xi_n\}$ form an orthonormal basis of $N(\Sigma)$.*

Proof of Proposition 2.4. $\Delta_T^{-1}S^{-1}$ is well defined and bounded by virtue of Assumption (i) and Lemma 2.3. For any given $f, g \in N(\Sigma)$, it holds that

$$\begin{aligned} - \int_{\Sigma} (\nabla_T \Delta_T^{-1} S^{-1} f) \cdot \nabla_T g \, do_x &= \int_{\Sigma} (S^{-1} f) g \, do_x \\ &= \int_{\Sigma} f (S^{-1} g) \, do_x = - \int_{\Sigma} \nabla_T f \cdot (\nabla_T \Delta_T^{-1} S^{-1} g) \, do_x \end{aligned}$$

Therefore, $\Delta_T^{-1}S^{-1}$ is self adjoint.

In order to establish compactness of $\Delta_T^{-1}S^{-1}$, we first fix a bounded sequence $g_i \in N(\Sigma)$. The image $u_i = \Delta_T^{-1}S^{-1}g_i$ is also a bounded sequence in $N(\Sigma)$. By Rellich's lemma, there exists subsequence u_{i_k} that is convergent in $L^2(\Sigma)$. Furthermore, we have

$$\int_{\Sigma} \nabla_T u_i \cdot \nabla_T u_j \, do_x = - \int_{\Sigma} S^{-1} g_i u_j \, do_x.$$

Thus $\nabla_T u_{i_k}$ converges componentwise in $L^2(\Sigma)$, which gives that u_{i_k} converges in $N(\Sigma)$.

The last statement follows immediately from the fact that S and Δ_T are bounded and invertible. Thus $\Delta_T^{-1}S^{-1}f \equiv 0$ immediately implies $f \equiv S \Delta_T 0 = 0$. \square

2.3. Proof of the spectral decomposition result.

Proof of Proposition 2.1. Let χ_j be the solution of (1.2). According to Lemma 2.2 we can write χ_j as a single layer potential with a density $\gamma \in L^2(\Sigma)$ that satisfy $\int_{\Sigma} \gamma \, do_x = 0$, viz.,

$$\chi_j = \mathbf{S}\gamma + C.$$

Using the invertibility of S we obtain that for $\xi = S\gamma \in N(\Sigma)$,

$$\chi_j = \mathbf{S}S^{-1}\xi + C.$$

Corollary 2.5 guarantees the existence of the expansion $\xi = \sum_k \alpha_j^k \xi_k$ with $\{\alpha_j^n\}_n \in \ell^2(\mathbb{C})$, which yields (2.5):

$$\chi_j = \mathbf{S}S^{-1} \left(\sum_k \alpha_j^k \xi_k \right) + C.$$

Identity (2.6) follows directly from substituting (2.5) into (1.2) and testing with $\psi = \mathbf{S}S^{-1}\xi_k$:

$$\begin{aligned} \eta(\omega) \int_{\Sigma} P_T(e_j) \cdot \nabla_T \bar{\xi}_k \, do_x &= \sum_n (\varepsilon \alpha_j^n / \lambda_n - \alpha_j^n \eta(\omega)) \int_{\Sigma} \nabla_T \xi_n \cdot \nabla_T \bar{\xi}_k \, do_x \\ &= \sum_n (\varepsilon \alpha_j^n / \lambda_n - \alpha_j^n \eta(\omega)) \delta_{kn} \\ &= \varepsilon \alpha_j^k / \lambda_k - \alpha_j^k \eta(\omega). \end{aligned}$$

Finally, Identity (2.7) follows from substituting (2.5) and (2.6) into (1.1). \square

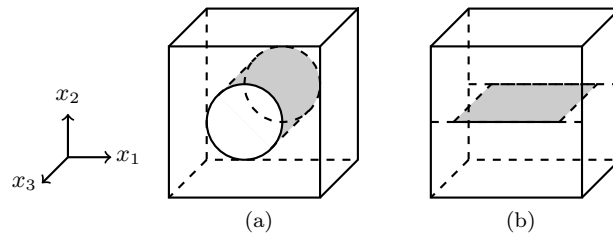


Figure 2: Prototypical geometries: (a) shows a nanotube configuration and (b) is a nanoribbon configuration. The diameter (in (a)) and the width (in (b)) was set to 0.8.

| order k | λ_k | $\left \int_{\Sigma} P_T(\mathbf{e}_1) \cdot \nabla_T \bar{\xi}_n \, do_x \right $ | λ_k | $\left \int_{\Sigma} P_T(\mathbf{e}_1) \cdot \nabla_T \bar{\xi}_n \, do_x \right $ |
|---------|-------------|---|-------------|---|
| 1 | 0.5924 | 1.1158 | 0.9873 | 0.8543 |
| 2 | 3.726 | 0.1077 | 5.314 | 0.1811 |
| 3 | 6.289 | 0.008194 | 9.283 | 0.1097 |
| 4 | 8.763 | 0.003574 | 13.22 | 0.07913 |
| 5 | 11.26 | 0.0002755 | 17.16 | 0.06194 |
| 6 | 13.76 | 0.00008546 | 25.02 | 0.04322 |
| 7 | 16.27 | 0.000009443 | 28.96 | 0.03755 |

(a) Nanotubes

(b) Nanoribbons

Table 1: Numerically computed spectrum and weight coefficients for the two geometries (Figure 2) using the computational approach outlined in Section 3(a): Table (a) shows results for the nanotube configuration. All roots have multiplicity 2; eigenvalues with weight 0 are omitted. Table (b) shows results for the nanoribbon geometry. Here all roots have multiplicity 1.

3. Computational platform. Proposition 2.1 enables a very efficient computation of the frequency response of a nanostructure by first solving a single geometric eigenvalue problem given by (2.4) approximately. Then, (2.7) can be invoked to characterize the frequency response of the permittivity tensor. We will illustrate this procedure in this section on two prototypical geometries shown in Figure 2: a nanotube configuration, which is a closed smooth surface; and a nanoribbon configuration which is an open surface with edges. We point out that due to the translation invariance in z -direction of both configuration, the corresponding corrector χ_3 vanishes. This implies that the corresponding cell problems (1.2) reduce to a two-dimensional problem, and that the third diagonal component of the effective conductivity tensor ε^{eff} is simply given by

$$\varepsilon_{33}^{\text{eff}} = \varepsilon - \eta(\omega) \int_{\Sigma} 1 \, do_x.$$

Due to symmetry we have $\varepsilon_{11}^{\text{eff}} = \varepsilon_{22}^{\text{eff}}$ for the nanotube configuration. In case of the nanoribbon geometry the averaging process in y -direction is trivial leading to $\varepsilon_{22}^{\text{eff}} = \varepsilon$. We thus only need to determine $\varepsilon_{11}^{\text{eff}}$ computationally in the following.

3.1. Numerical computation of the geometric spectrum. In order to approximate (2.4) numerically we recast the eigenvalue problem in variational form (1.3): Find $\varphi_n \in \mathcal{H}$ and $\lambda_n \in \mathbb{R}$ such that

$$\lambda_n \int_Y \nabla \varphi_n(\mathbf{x}) \cdot \nabla \bar{\psi}(\mathbf{x}) \, dx = \int_{\Sigma} \nabla_T \varphi_n(\mathbf{x}) \cdot \nabla_T \bar{\psi}(\mathbf{x}) \, do_x, \quad \forall \psi \in \mathcal{H}.$$

This eigenvalue problem can be efficiently approximated with a finite element discretization which we will quickly outline. We use the finite element toolkit deal.II [2, 3]. To achieve a good numerical convergence order we use unstructured quadrilateral meshes \mathcal{T}_h for both geometries that are fitted to the curved hypersurface Σ by aligning element boundaries with the hypersurface [10] and discretize with high-order Lagrange elements. Let $\{\psi_i^h\}_{i \in \{1:\mathcal{N}\}}$ be the nodal basis of the Lagrange ansatz. We can then define the usual stiffness matrix $M = (m_{ij})$

$$m_{ij} = \sum_{Q \in \mathcal{T}_h} \int_Q \nabla \psi_j^h(\mathbf{x}) \cdot \nabla \psi_i^h(\mathbf{x}) \, dx.$$

The boundary term requires a modification because the trace $\nabla_T \psi_i^h$ is not single-valued and only defined on an individual cell of the mesh. We thus define a matrix $S = (s_{ij})$ by averaging both cell contributions to the gradient:

$$s_{ij} = \sum_{Q \in \mathcal{T}_h} \frac{1}{2} \int_{\partial Q} \nabla_T \psi_j^h(\mathbf{x}) \cdot \nabla_T \psi_i^h(\mathbf{x}) \, do_x.$$

We can then compute an approximate spectrum λ_n^h and discrete eigenfunctions $\xi_n^h = \sum_i \Xi_{n,i}^h \psi_i^h$ by solving the matrix eigenvalue problem

$$(S + bM) \Xi_n^h = \tilde{\lambda}_n^h M \Xi_n^h$$

with an eigenvalue solver, such as SLEPc [8]. Here, $b > 0$ is a suitably chosen Moebius parameter. The original eigenvalue is recovered via by setting $\lambda_n^h = \tilde{\lambda}_n^h - b$. We briefly comment on one crucial subtlety of this approach. The discrete eigenvectors Ξ_n^h are orthonormal with respect to the inner product $\langle M \cdot, \cdot \rangle$ due to the mass matrix M appearing on the right hand side. This inner product is the discrete analogue of $\int_Y \nabla \cdot \nabla \cdot dx$ and not the normalization we used in Proposition 2.1. This does not change the computed eigenvalues but has an effect on the surface integrals that have to be computed next; see Proposition A.5 and the discussion in Appendix A. This can be easily cured by scaling the surface integrals appropriately by $1/\sqrt{\lambda_n^h}$, cf. Equations (2.7) and (A.3). We report numerical results for the two geometries (Figure 2) in Table 1. The decay rate of the weight coefficients $\left| \int_{\Sigma} P_T(\mathbf{e}_1) \cdot \nabla_T \bar{\xi}_n \, do_x \right|$ deserves a short discussion. The rapid convergence of the coefficients to zero in case of nanotubes is owed to the regularity of Σ and the absence of interior edges. The eigenvalues and eigenfunctions of the nanotube geometry can be explicitly computed when the periodic boundary condition on Y is replaced by an infinite domain and the Sommerfeld radiation condition (see Appendix B). In this case only the first order, viz. $k = 1$, has a nonzero contribution to the resonance. The rapid decay of the weight coefficients in our numerical result for the periodic case is qualitatively in agreement with this observation. Due to the singularities at the corners of the nanoribbon geometry [19], it is not surprising that the decay rate of the weight coefficients is limited.

An n -th order numerical approximation of the effective permittivity tensor can be constructed by invoking a discrete counterpart of (2.7):

$$(3.1) \quad \varepsilon_{11}^{\text{app}}(\omega) = \varepsilon - \eta(\omega) \sum_{Q \in \mathcal{T}_h} \sum_{\partial Q \cap \Sigma} P_T(\mathbf{e}_1) \cdot P_T(\mathbf{e}_1) \, d\sigma_x \\ - \sum_{k=1}^n \frac{\lambda_k^h \eta^2(\omega)}{\varepsilon - \lambda_k^h \eta(\omega)} \left| \sum_{Q \in \mathcal{T}_h} \sum_{\partial Q \cap \Sigma} P_T(\mathbf{e}_1) \cdot \nabla_T \xi_n^h \, d\sigma_x \right|^2.$$

3.2. Comparison. Choosing $\varepsilon = 1$, we compute a reference frequency response of $\varepsilon_{11}^{\text{eff}}(\omega)$ by finely sampling over a set frequency range $0 < \omega < 0.5$ and performing a complete direct numerical computation of the cell problem for selected frequencies: For every chosen angular frequency ω we first determine the corrector by solving (1.2) with a finite-element code [13] up to a suitable resolution (about 110 k unknowns for the nanotube configuration, and about 130 k unknowns for the nanoribbon configuration). The result is plotted in Figures 3a and 4a. In both plots about 700 frequencies were chosen adaptively.

We then compare a second order approximation $\varepsilon_{11}^{\text{app}}$ by using (3.1) with $n = 2$ against the direct numerical computation graphically in Figures 3a and 4a. For the chosen frequency range we observe an excellent agreement of the approximative permittivity $\varepsilon_{11}^{\text{app}}$ with the reference computation in the “eyeball” norm.

A more detailed comparison of the frequency behavior of the relative error between both computations is given in Figures 3b and 4b, where also the dependence of the error on the order n of the approximation (3.1) is visualized. On average we observe a relative error of less than 1%. We note that the maxima in the relative error naturally occur at corresponding Lorentz resonances and are dominated by the approximation error of the underlying finite element simulations. We observe an exponential decay of the relative error as a function of approximation order for the smooth nanotubes geometry (see Figure 3b). The corresponding convergence behavior for nanoribbons as shown in Figure 4b is significantly slower. This is owed to the fact that the edges in the nanoribbon geometry cause singularity in the solution of the cell problems thus limiting the approximation order [19].

4. Conclusion. In this paper, we analyzed the sharp Lorentz resonances in plasmonic crystals that consist of 2D nano dielectric inclusions embedded in a nonmagnetic bulk. From the corrector field found in a rigorous homogenization theory (1.2), we derived an analytic expansion formula for the effective permittivity (1.4). This formula decouples the local geometric resonances and the material properties, and thus enables a very efficient approximation to compute the frequency response. This formula holds for inclusions of a large family of geometries, including closed surfaces (as shown in Sec. 2) and open surfaces that can be completed into closed surfaces as shown in Appendix A.

We observe that up to a constant factor, the k th Lorentz resonance is described by

$$\frac{\lambda_n \eta^2(\omega)}{\varepsilon - \lambda_n \eta(\omega)} \sim \frac{\varepsilon \lambda_n \omega_p^2 (\omega - i/\tau)}{\omega (\omega^2 + 1/\tau^2)}.$$

We have also observed that a crucial quantity that determines the convergence speed of this expansion is the decay rate of a weight factor

$$\left| \int_{\Sigma} P_T(\mathbf{e}_1) \cdot \nabla_T \bar{\xi}_n \, d\sigma_x \right|^2.$$

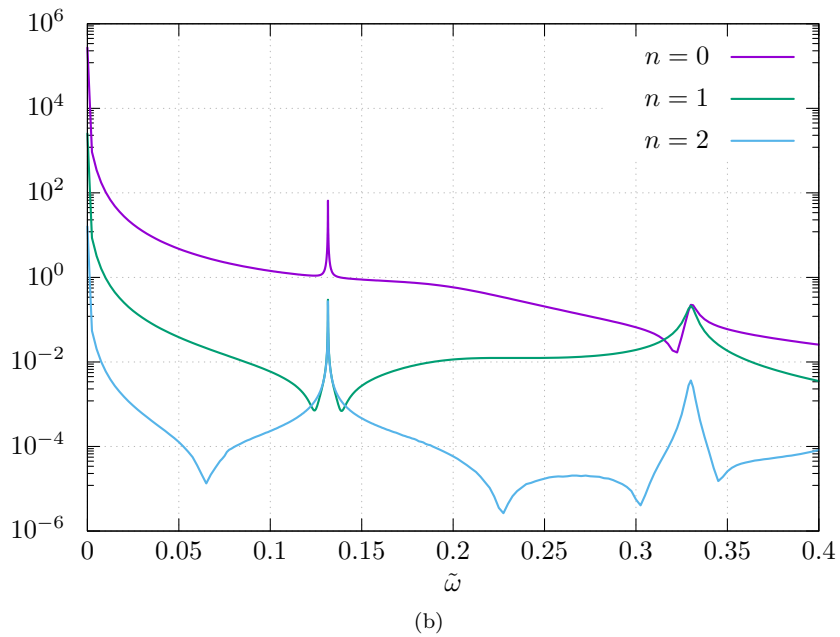
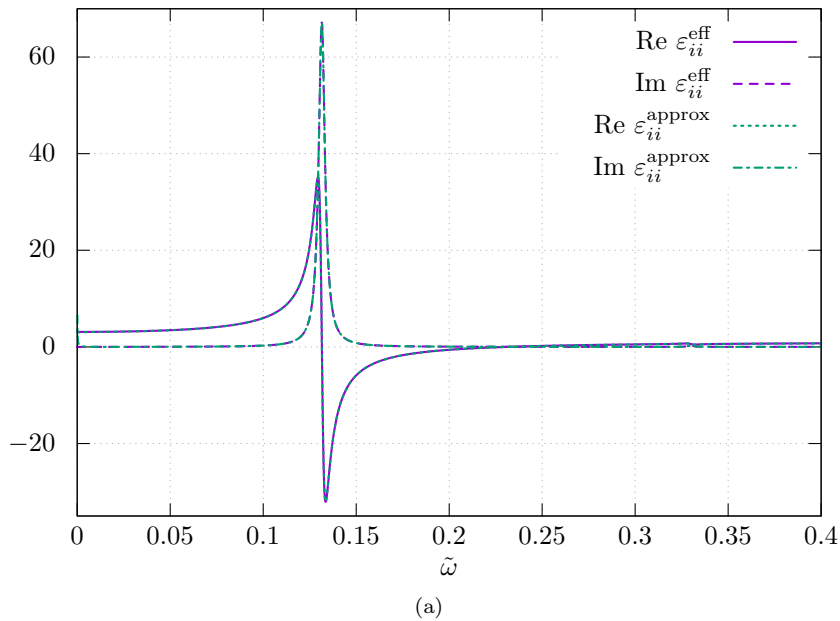


Figure 3: (a) Frequency response of $\varepsilon_{ii}^{\text{eff}}(\omega)$, $i = 1, 2$, for the nanotube configuration: The solid (real part) and dashed lines (imaginary part) are computed with (1.1) by solving problem (1.2) for every ω ; the dotted and dash-dotted lines are computed by formula (2.7) truncated at $n = 2$. (b) The corresponding relative error as a function of frequency.

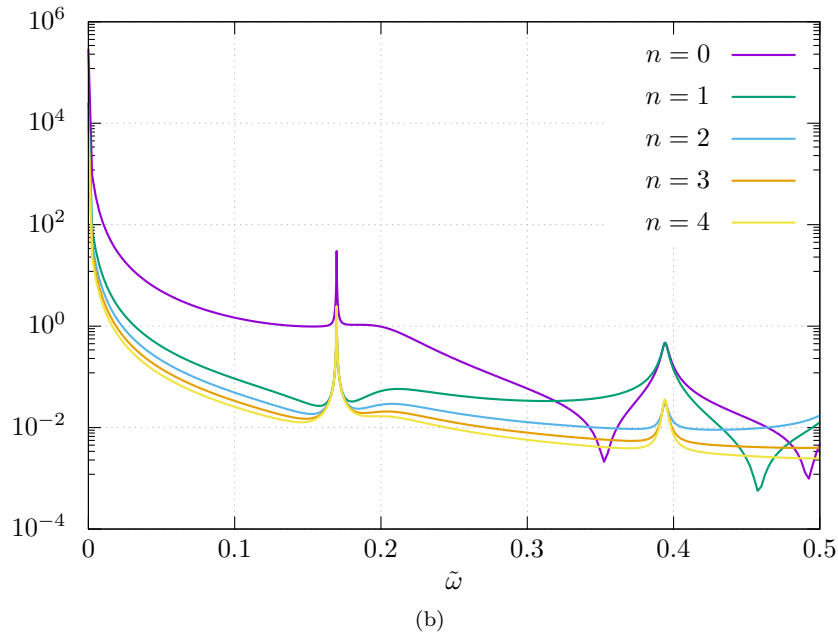
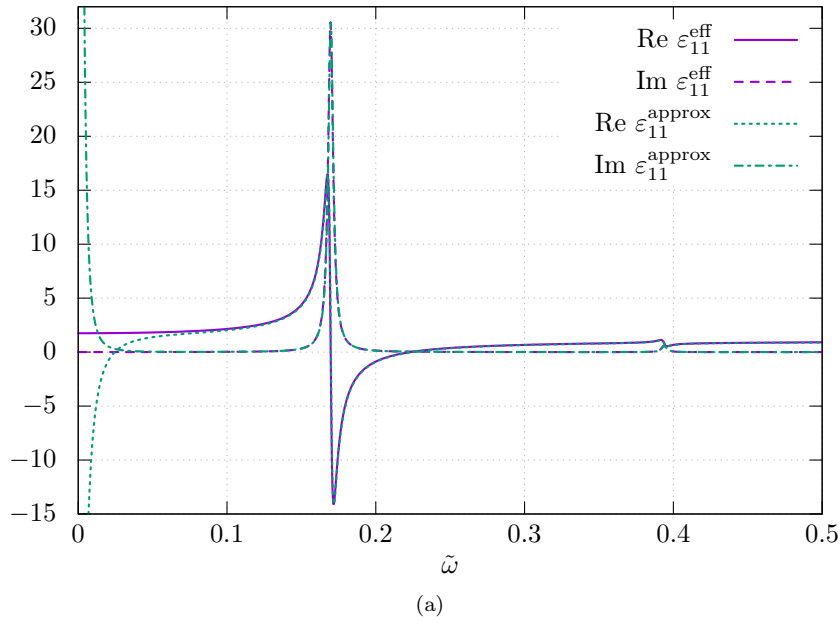


Figure 4: (a) Frequency response of $\varepsilon_{11}^{\text{eff}}(\omega)$, for the nanoribbon configuration: The solid (real part) and dashed lines (imaginary part) are computed with (1.1) by solving problem (1.2) for every ω ; the dotted and dash-dotted lines are computed by formula (2.7) truncated at $n = 2$. (b) The corresponding relative error as a function of frequency.

The decay rate depends on the smoothness of the corrector, i. e., whether singularities due to roughness or edges are present in the cell problem. We have demonstrated that our spectral decomposition approach offers a significant saving in computational resources because only one frequency-independent geometric eigenvalue problem has to be computed, in contrast to computing the corrector field for a huge number of fixed frequencies.

Appendix A. Spectral decomposition on open surfaces.

When Σ is an open surface, in the sense that Σ has edges in the interior of Y , the property in Sec. 22.1, $S : L^2(\Sigma) \rightarrow H^1(\Sigma)$ is invertible, no longer holds. One counter example is that in two dimensional space, the non-periodic single layer potential maps $\frac{1}{\sqrt{a-x^2}}$ to a constant function on the interval $[-a, a]$ [26]. This means that we cannot write $\chi_j = \mathbf{S}\gamma + C$ for some $\gamma \in L^2(\Sigma)$. However, this representation is valid for γ in a proper fractional Sobolev space. Thus we go to fractional Sobolev spaces to obtain the expansion (1.4). In this appendix, we list the modifications to Sec. 2, assuming that Σ can be completed into a closed smooth surface Σ_* .

A.1. Sobolev spaces on open surfaces. We give a definition of Sobolev spaces defined on open surfaces following the notations in [14]. First, on a closed $C^{k,1}$ surface Σ_* in \mathbb{R}^n , where $k \geq 0$ and $n > 0$ are integers, $H^s(\Sigma_*)$ is defined through charts and the Fourier transform for $s \in [-k-1, k+1]$ [14, P.98].

Let Σ be an open subset of Σ_* . For every real number $s \in \mathbb{R}$, we define

$$\begin{aligned} H^s(\Sigma) &:= \left\{ f : \Sigma \rightarrow \mathbb{C} \mid f \text{ has an extension } \tilde{f} \in H^s(\Sigma_*) \right\}, \\ \tilde{H}^s(\Sigma) &:= \text{closure of } C_0^\infty(\Sigma) \text{ in } H^s(\Sigma_*). \end{aligned}$$

It is shown in [14, Thm. 3.14, Thm. 3.29, Thm. 3.30] that when Σ is a Lipschitz subset of Σ_* , for all $s \in \mathbb{R}$,

$$\begin{aligned} (\tilde{H}^s(\Sigma))' &= H^{-s}(\Sigma), \\ (H^s(\Sigma))' &= \tilde{H}^{-s}(\Sigma), \\ \tilde{H}^s(\Sigma) &= \{f \in H^s(\Sigma_*) \mid \text{supp } f \subset \bar{\Sigma}\}, \end{aligned}$$

and for an integer $m \in [0, k+1]$,

$$\begin{aligned} H^m(\Sigma) &= \{f : \Sigma \rightarrow \mathbb{C} \mid \\ & f \text{ and its weak tangential derivatives up to order } m \text{ are in } L^2(\Sigma)\}. \end{aligned}$$

Note that the above defined $H^s(\Sigma)$ and $\tilde{H}^{-s}(\Sigma)$ for $s \geq 0$ are the same as those defined in [20, 25].

A.2. Spectral decomposition. Now we state the lemmas parallel to the ones in Sec. 2. Since χ_j belongs to $H^1(Y)$, its distributional Laplacian is 0, and $[\partial_n \chi_j] = 0$ on $\Sigma_* \setminus \Sigma$, we obtain the standard result that

LEMMA A.1. *For the corrector χ_j solving (1.2), there is a unique $\gamma \in \tilde{H}^{-1/2}(\Sigma, \mathbb{C})$ and a unique constant C , such that*

$$\chi_j = \mathbf{S}\gamma + C.$$

This γ satisfies that $\int_\Sigma \gamma \, d\sigma_x = 0$.

The mapping property of S on $\tilde{H}^{-1/2}(\Sigma)$ is given by

LEMMA A.2 ([20, 25]). *The single layer operator $S : \tilde{H}^{-1/2}(\Sigma) \rightarrow H^{1/2}(\Sigma)$ is bijective.*

The proper Hilbert space to consider becomes

$$(A.1) \quad \mathcal{N}(\Sigma) := \left\{ f \in H^{1/2}(\Sigma), \langle S^{-1}f, 1 \rangle_\Sigma = 0 \right\},$$

equipped with the inner product is $\langle -S^{-1}\xi, \eta \rangle_\Sigma$. Here, $\langle \cdot, \cdot \rangle_\Sigma$ is the $L^2(\Sigma)$ pairing, and we'll refer to $\langle -S^{-1}\xi, \eta \rangle_\Sigma$ as the S^{-1} inner product.

On this space, we consider the following inverse of Δ_T .

LEMMA A.3 (A particular inverse of Δ_T). *For $f \in \tilde{H}^{-1}(\Sigma)$ with $\langle f, 1 \rangle_\Sigma = 0$, there exists a unique $g \in H^1(\Sigma)$ with $\langle S^{-1}g, 1 \rangle_\Sigma = 0$, such that*

$$(A.2) \quad -\langle f, \psi \rangle_\Sigma = \int_\Sigma \nabla_T g \cdot \nabla_T \bar{\psi} \, do_x, \quad \text{for all } \psi \in H^1(\Sigma).$$

Moreover, the solution g of (A.2) is bounded, $\|g\|_{H^1(\Sigma)} \leq C\|f\|_{\tilde{H}^{-1}(\Sigma)}$. We will denote this solution operator by Δ_T^{-1} .

Proof. Given $f \in \tilde{H}^{-1}(\Sigma)$ with $\langle f, 1 \rangle_\Sigma = 0$, it follows from standard elliptic equation theory that there exists a unique $\tilde{g} \in H^1(\Sigma)$ with $\langle \tilde{g}, 1 \rangle_\Sigma = 0$, such that

$$\begin{aligned} -\int_\Sigma f \bar{\psi} \, do_x &= \int_\Sigma \nabla_T \tilde{g} \cdot \nabla_T \bar{\psi} \, do_x \quad \forall \psi \in H^1(\Sigma), \\ \|\tilde{g}\|_{H^1(\Sigma)} &\leq C\|f\|_{\tilde{H}^{-1}(\Sigma)}. \end{aligned}$$

Now let $g_0 = S^{-1}1 \in \tilde{H}^{-1/2}(\Sigma)$ and define the constant

$$C(\tilde{g}) := \langle S^{-1}\tilde{g}, 1 \rangle_\Sigma / \langle S^{-1}1, 1 \rangle_\Sigma = \langle \tilde{g}, g_0 \rangle_\Sigma / \langle 1, g_0 \rangle_\Sigma.$$

The function $g := \tilde{g} - C(\tilde{g})$ obviously solves (A.2) and by construction $\langle S^{-1}g, 1 \rangle_\Sigma = 0$. The bound follows from

$$\|C(\tilde{g})\|_{H^1} = \|C(\tilde{g})\|_{L^2} \leq C|\langle S^{-1}\tilde{g}, 1 \rangle_\Sigma| \leq C\|S^{-1}\tilde{g}\|_{L^2} \leq C\|\tilde{g}\|_{H^1} \leq C\|f\|_{\tilde{H}^{-1}}. \quad \square$$

Since $\Delta_T^{-1}S^{-1}$ maps $\mathcal{N}(\Sigma) \subset H^{1/2}(\Sigma)$ into $H^1(\Sigma) \subset\subset H^{1/2}(\Sigma)$, it's easy to verify:

PROPOSITION A.4. *The operator*

$$\Delta_T^{-1}S^{-1} : \mathcal{N}(\Sigma) \rightarrow \mathcal{N}(\Sigma)$$

is compact and self-adjoint with respect to the S^{-1} pairing. Here Δ_T^{-1} is the particular operator defined in Lemma A.3. Moreover,

$$\ker(\Delta_T^{-1}S^{-1}) = \{0\}.$$

Finally, the result analogue to Proposition 2.1 reads

PROPOSITION A.5 (Spectral decomposition for open surfaces). *Let χ_j be the solution of the cell problem (1.2). Let $\{\xi_n, \lambda_n^{-1}\}_n$ be the orthonormal eigen-system of the operator $\Delta_T S$ in the space $\mathcal{N}(\Sigma)$. Then*

$$\chi_j = \mathbf{S}S^{-1} \left(\sum_n \alpha_j^n \xi_n \right) + C,$$

where C is a constant and

$$\alpha_j^n = \frac{\eta(\omega)}{\varepsilon - \lambda_n \eta(\omega)} \int_{\Sigma} P_T(\mathbf{e}_j) \cdot \nabla_T \bar{\xi}_k \, d\mathbf{o}_x.$$

Furthermore,

$$\begin{aligned} \text{(A.3)} \quad \varepsilon_{ij}^{\text{eff}} &= \varepsilon \delta_{ij} - \eta(\omega) \int_{\Sigma} P_T(\mathbf{e}_j) \cdot P_T(\mathbf{e}_i) \, d\mathbf{o}_x \\ &\quad - \sum_n \frac{\eta^2(\omega)}{\varepsilon - \lambda_n \eta(\omega)} \int_{\Sigma} P_T(\mathbf{e}_j) \cdot \nabla_T \bar{\xi}_n \, d\mathbf{o}_x \int_{\Sigma} \nabla_T \xi_n \cdot P_T(\mathbf{e}_i) \, d\mathbf{o}_x. \end{aligned}$$

Note that the S^{-1} inner product gives a different normalization of ξ_n hence different α_j^n values. In terms of the scaled function $\tilde{\xi}_k := \frac{\xi_k}{\sqrt{|\lambda_k|}}$, (1.3) is satisfied and the expansion (A.3) takes the same form as (1.4).

Appendix B. Explicitly computable examples.

In this appendix, we explicitly compute the eigensystem of $\Delta_T^{-1} S^{-1}$ on two *non-periodic* geometries in \mathbb{R}^3 . These examples qualitatively illustrate the corresponding periodic geometries, when the inclusions are far apart from each other. On spheres and circular cylinders in \mathbb{R}^3 , the eigensystem of $\Delta_T S$ are explicitly known. This is because Δ_T and S separately have explicit eigensystems, and they share eigenfunctions. Note that the only manifolds on which the Laplace-Beltrami operator has explicit eigensystems are n -spheres, n -tori and Heisenberg groups.

B.1. Circular cylinder. Let Σ be a cylinder with a circular cross section of radius a . The corresponding periodic geometry is the nanotube structure considered numerically in Sec. 3. We will abuse notation by denoting the cross sections of all quantities by the same notation, since all quantities are invariant along the axis of the cylinder. A basis for mean zero $L^2(\Sigma)$ functions is $\{e^{in\theta}, n \neq 0\}$. This is also a set of simultaneous eigen functions for Δ_T and S :

$$\Delta_T e^{in\theta} = -\frac{n^2}{a^2} e^{in\theta}, \quad S e^{in\theta} = -\frac{a}{2n} e^{in\theta}.$$

Thus the eigen system for (2.4) normalized in the $\|\nabla_T \cdot\|_{\Sigma}$ norm is

$$\lambda_n = \frac{n}{2a}, \quad \xi_n^i = \begin{cases} \frac{1}{n} \sqrt{\frac{a}{\pi}} \cos(n\theta), & i = 1 \\ \frac{1}{n} \sqrt{\frac{a}{\pi}} \sin(n\theta), & i = 2 \end{cases}, \quad n \geq 1.$$

Using $P_T(\mathbf{e}_1) = -\hat{\theta} \sin \theta$ and $\nabla_T = \hat{\theta}^1 \partial_{\theta}$, we obtain

$$\int_{\Sigma} P_T(\mathbf{e}_1) \cdot \nabla_T \bar{\xi}_n^i \, d\mathbf{o}_x = \begin{cases} \sqrt{\pi a}, & n = 1, i = 1, \\ 0, & \text{otherwise.} \end{cases}$$

Note that the for the corresponding periodic geometry, the factor $\int_{\Sigma} P_T(\mathbf{e}_1) \cdot \nabla_T \bar{\xi}_n^i \, d\mathbf{o}_x$ in Table 1 decays, instead of falling to zero abruptly. This is due to the effect from other cylinders in the array. The decay becomes faster when the size of the cylinder relative to the cell becomes smaller.

B.2. Sphere. Let Σ be a sphere of radius a . A basis for mean zero $L^2(\Sigma)$ functions is the set of spherical harmonic functions $\{Y_n^m, n \geq 1, -n \leq m \leq n\}$. This is also a set of simultaneous eigenfunctions for Δ_T and S :

$$\Delta_T Y_n^m = -\frac{n(n+1)}{a^2} Y_n^m, \quad S Y_{n,m} = -\frac{a}{2n+1} Y_{n,m}.$$

Thus the eigensystem for (2.4) is normalized in the $\|\nabla_T \cdot\|_\Sigma$ norm is

$$\lambda_n = \frac{n(n+1)}{a(2n+1)}, \quad \xi_n^i = \frac{1}{\sqrt{n(n+1)}} Y_{n,m}, \quad n \geq 1, -n \leq m \leq n.$$

Using $P_T(\mathbf{e}_1) = \hat{\theta} \cos \theta \cos \phi - \hat{\phi} \sin \phi$, $\nabla_T = \hat{\theta} \frac{1}{a} \partial_\theta + \hat{\phi} \frac{1}{a \sin \theta} \partial_\phi$ and the recurrence relations for the associated Legendre polynomials, we obtain

$$\int_\Sigma P_T(\mathbf{e}_1) \cdot \nabla_T \bar{\xi}_n^i \, d\sigma_x = \begin{cases} \mp 2a \sqrt{\frac{\pi}{3}}, & n=1, m=\pm 1, \\ 0, & \text{otherwise.} \end{cases}$$

Acknowledgments. RL acknowledges partial support by the NSF under grant DMS-1921707 and 1813698, MM acknowledges partial support by the NSF under grant DMS-1912847.

References.

- [1] Y. AMIRAT AND V. V. SHELUKHIN, *Homogenization of time harmonic Maxwell equations: the effect of interfacial currents*, *Mathematical Methods in the Applied Sciences*, 40 (2017), pp. 3140–3162.
- [2] D. ARNDT, W. BANGERTH, B. BLAIS, T. C. CLEVINGER, M. FEHLING, A. V. GRAYVER, T. HEISTER, L. HELTAI, M. KRONBICHLER, P. MUNCH, M. MAIER, J.-P. PELTERET, R. RASTAK, B. TURCK SIN, Z. WANG, AND D. WELLS, *The deal.II Library, Version 9.2*, *Journal of Numerical Mathematics*, accepted (2020), <https://doi.org/https://doi.org/10.1515/jnma-2020-0043>.
- [3] D. ARNDT, W. BANGERTH, D. DAVYDOV, T. HEISTER, L. HELTAI, M. KRONBICHLER, M. MAIER, J.-P. PELTERET, B. TURCK SIN, AND D. WELLS, *The deal.II finite element library: design, features, and insights*, *Computers & Mathematics with Applications*, accepted (2020), <https://doi.org/10.1016/j.camwa.2020.02.022>.
- [4] D. J. BERGMAN, *The dielectric constant of a composite material - a problem in classical physics.*, *Physics Reports*, 43 (1978), pp. 377–407.
- [5] Y. CHEN AND R. LIPTON, *Resonance and double negative behavior in metamaterials*, *Archive for Rational Mechanics and Analysis*, 209 (2013), pp. 835–868.
- [6] D. GILBARG AND N. S. TRUDINGER, *Elliptic partial differential equations of second order*, Springer, 2015.
- [7] K. GOLDEN AND G. PAPANICOLAOU, *Bounds for effective parameters of heterogeneous media by analytic continuation*, *Commun. Math. Phys.*, 90 (1983), pp. 473–491.
- [8] V. HERNANDEZ, J. E. ROMAN, AND V. VIDAL, *SLEPc: A scalable and flexible toolkit for the solution of eigenvalue problems*, *ACM Trans. Math. Software*, 31 (2005), pp. 351–362.
- [9] R. LIPTON AND R. VIATOR, *Bloch waves in crystals and periodic high contrast media*, *ESAIM Mathematical Modeling and Numerical Analysis*, 51 (2017), pp. 889–918.

- [10] M. MAIER, D. MARGETIS, AND M. LUSKIN, *Dipole excitation of surface plasmon on a conducting sheet: finite element approximation and validation*, J. Comp. Phys., 339 (2017), pp. 126–145, <https://doi.org/10.1016/j.jcp.2017.03.014>.
- [11] M. MAIER, D. MARGETIS, AND M. LUSKIN, *Finite-size effects in wave transmission through plasmonic crystals: A tale of two scales*, Submitted, (2020).
- [12] M. MAIER, D. MARGETIS, AND A. MELLET, *Homogenization of time-harmonic maxwell's equations in nonhomogeneous plasmonic structures*, Journal of Computational and Applied Mathematics, (2020), p. 112909.
- [13] M. MAIER, M. MATTHEAKIS, E. KAXIRAS, M. LUSKIN, AND D. MARGETIS, *Homogenization of plasmonic crystals: Seeking the epsilon-near-zero effect*, Proceedings of the Royal Society A: Mathematical, Physical, and Engineering Sciences, 475 (2019), p. 20190220, <https://doi.org/10.1098/rspa.2019.0220>, <https://arxiv.org/abs/1809.08276>.
- [14] W. MCLEAN, *Strongly elliptic systems and boundary integral equations*, Cambridge University Press, 2000.
- [15] R. C. MCPHEDRAN AND G. W. MILTON, *Bounds and exact theories for transport properties of inhomogeneous media*, Applied Physics A., 26 (1981), pp. 207–220.
- [16] G. W. MILTON, *Bounds on the complex permittivity of a two-component composite material*, J. Appl. Phys., 52 (1981), pp. 5286–5293.
- [17] G. W. MILTON, *The Theory of Composites*, Cambridge University Press, Cambridge, 2002.
- [18] A. PORS, O. ALBREKTSSEN, I. RADKO, AND S. BOZHEVONLNYI, *A review of gap-surface plasmon metasurfaces: fundamentals and applications*, Sci. Rep., 3 (2013), p. 2155.
- [19] B. H. RANNACHER, R., *Extrapolation techniques for reducing the pollution effect of reentrant corners in the finite element method.*, Numerische Mathematik, 52 (1987/88), pp. 539–564, <http://eudml.org/doc/133252>.
- [20] E. P. STEPHAN, *Boundary integral equations for screen problems in \mathbb{R}^3* , Integral Equations and Operator Theory, 10 (1987), pp. 236–257.
- [21] R. TAUBERT, D. DREGELY, T. STROUCKEN, A. CHRIST, AND H. GIESSEN, *Octave-wide photonic band gap in three-dimensional plasmonic bragg structures and limitations of radiative coupling*, Nature Communications, 3 (2012), p. 691, <https://doi.org/10.1038/ncomms1694>.
- [22] N. WELLANDER, *Homogenization of the Maxwell equations: Case i. linear theory*, Applications of Mathematics, 46 (2001), pp. 29–51.
- [23] N. WELLANDER, *Homogenization of the Maxwell equations: Case ii. nonlinear conductivity*, Applications of Mathematics, 47 (2002), pp. 255–283.
- [24] N. WELLANDER AND G. KRISTENSSON, *Homogenization of the Maxwell equations at fixed frequency*, SIAM Journal on Applied Mathematics, 64 (2003), pp. 170–195.
- [25] W. L. WENDLAND, E. STEPHAN, DARMSTADT, AND G. C. HSIAO, *On the integral equation method for the plane mixed boundary value problem of the laplacian*, Mathematical Methods in the Applied Sciences, 1 (1979), pp. 265–321.
- [26] I. H. S. Y. YAN, *On integral equations of the first kind with logarithmic kernels*, Journal of integral equations and applications, 1 (1988), pp. 549–579.
- [27] Y. ZHAO AND A. ALÛ, *Manipulating light polarization with ultrathin plasmonic metasurfaces*, Physical Review B, 84 (2011), p. 205428.
- [28] Y. ZHAO, X.-X. LIU, AND A. ALÛ, *Recent advances on optical metasurfaces*, Journal of Optics, 16 (2014), p. 123001.